

Article

Combined State of Charge and State of Energy Estimation for Echelon-Use Lithium-Ion Battery Based on Adaptive Extended Kalman Filter

Enguang Hou ^{1,2}, Zhen Wang ¹, Xiaopeng Zhang ³, Zhixue Wang ^{1,*}, Xin Qiao ¹ and Yun Zhang ¹

¹ School of Rail Transportation, Shandong Jiao Tong University, Jinan 250357, China; houenguang@mail.sdu.edu.cn (E.H.); 215043@sdjtu.edu.cn (X.Q.); 215033@sdjtu.edu.cn (Y.Z.)

² School of Electrical Engineering, Shandong University, Jinan 250061, China

³ Langchao Electronic Industry Group Corp., Jinan 250101, China; zhangxpeng@inspur.com

* Correspondence: 215035@sdjtu.edu.cn

Abstract: To ensure the safety and reliability of an echelon-use lithium-ion battery (EULIB), the performance of a EULIB is accurately reflected. This paper presents a method of estimating the combined state of energy (SOE) and state of charge (SOC). First, aiming to improve the accuracy of the SOE and SOC estimation, a third-order resistor-capacitance equivalent model (TRCEM) of a EULIB is established. Second, long short-term memory (LSTM) is introduced to optimize the Ohmic internal resistance (OIR), actual energy (AE), and actual capacity (AC) parameters in real time to improve the accuracy of the model. Third, in the process of the SOE and SOC estimation, the observation noise equation and process noise equation are updated iteratively to make adaptive corrections and enhance the adaptive ability. Finally, an SOE and SOC estimation method based on LSTM optimization and an adaptive extended Kalman filter (AEKF) is established. In simulation experiments, when the capacity decays to 90%, 60% and 30% of the rated capacity, regardless of whether the initial value is consistent with the actual value, the values of the SOE and SOC estimation can track the actual value with strong adaptive ability, and the estimated error is less than 1.19%, indicating that the algorithm has a high level of accuracy. The method presented in this paper provides a new perspective for estimating the SOE and SOC of a EULIB.



Citation: Hou, E.; Wang, Z.; Zhang, X.; Wang, Z.; Qiao, X.; Zhang, Y. Combined State of Charge and State of Energy Estimation for Echelon-Use Lithium-Ion Battery Based on Adaptive Extended Kalman Filter. *Batteries* **2023**, *9*, 362. <https://doi.org/10.3390/batteries9070362>

Academic Editor: Matthieu Dubarry

Received: 19 May 2023

Revised: 20 June 2023

Accepted: 4 July 2023

Published: 6 July 2023



Copyright: © 2023 by the authors. Licensee MDPI, Basel, Switzerland. This article is an open access article distributed under the terms and conditions of the Creative Commons Attribution (CC BY) license (<https://creativecommons.org/licenses/by/4.0/>).

1. Introduction

Owing to the energy crisis and environmental pollution, new energy has attracted an increasing amount of attention. Lithium-ion batteries (LIBs) are widely used in electric vehicles and energy storage systems due to the advantages of having high energies, high power densities and environmental protection properties [1–3].

With the wide application of LIBs, echelon utilization has become a key method for resolving the problem of retired batteries. An echelon-use lithium-ion battery (EULIB) refers to a power LIB with a capacity of less than 80%, and EULIBs were shown to still have high discharge abilities which can be used for backup power supply and other occasions [4].

State of energy (SOE) and state of charge (SOC) are important parameters of a EULIB which ensure the safe, reliable, and efficient operation of a EULIB. Due to the degradation of EULIB performance and the poor consistency of the working voltage (WV) of lithium batteries, it is difficult to accurately characterize the state of a EULIB via its SOC only. Therefore, SOE estimation is introduced, and the combined parameters of SOC and SOE are used to characterize the state of the EULIB.

To improve a EULIB's performance, an algorithm for a high-accuracy estimation of the SOE and SOC is needed [3]. The SOE and SOC estimation methods for EULIBs are shown in Figure 1: integral, data-driven and model-based methods [5].

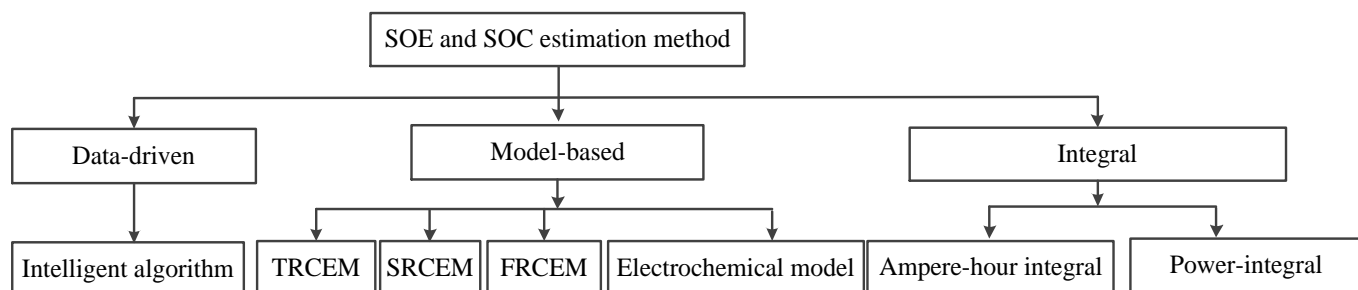


Figure 1. SOE and SOC estimation method.

A common method for estimating the SOE and SOC is the integral method [6,7]. On one hand, the integral method needs to provide an accurate initial value; otherwise, it is easy to introduce an initial error. On the other hand, this method is an open loop which lacks the ability for feedback correction. With an increase in time, the cumulative error will become larger and larger.

The equivalent circuit model is adopted in the model-based method, which mainly includes the electrochemical model, first-order resistor-capacitance equivalent model (FRCEM), second-order resistor-capacitance equivalent model (SRCEM), third-order resistor-capacitance equivalent model (TRCEM), and so on. In Refs. [8,9], an electrochemical model was used which achieved a good balance between accuracy and computational cost. Ref. [3] proposed a joint method based on a dual H infinity filter. In dynamic operation, estimators with different time scales were used based on an FRCEM, and the SOE and SOC estimation errors were less than 2%. In Ref. [10], two FRCEMs were established online via an extended Kalman filter (EKF). The prediction accuracy was verified through a complex driving simulation. The SRCEM has the advantages of a simple model and small computational costs, but its estimation accuracy is not high. To further improve the estimation accuracy, the SRCEM has been widely investigated. Ref. [11] proposed a joint method and estimated a LIB's state under dynamic working conditions. In Ref. [12], a method was proposed based on an SRCEM which could estimate a battery's SOC, SOE, state of power (SOP) and state of health (SOH) simultaneously. The results of dynamic load experiments indicated that it has a high level of precision and better robustness. The SRCEM, based on the FRCEM, improves the accuracy of SOE estimations but does not fully characterize the charging and discharging performance of an LIB. The TRCEM is widely used to estimate the SOC, SOP, SOH, SOE and other parameters and can not only improve the accuracies of the parameters but also can characterize the performance of the LIB well.

With the continuous development of machine learning, an increasing number of people pay attention to data-driven methods [13]. Generally, data-driven methods, for example, genetic algorithms [14], the gated recurrent unit (GRU), convolutional neural networks (CNNs), and long short-term memory (LSTM) [15–17], are widely used to estimate the SOE and SOC. In Ref. [18], a soft sensor was built based on a feedforward neural network. The proposed method attained a higher prediction accuracy. In Refs. [19,20], researchers used the GRU method and improved method and achieved good results. Ref. [21] proposed a data-driven method based on LSTM to jointly estimate the SOC and SOE. The dynamic cycle experiment showed that the method is accurate. In Refs. [22,23], an LSTM combined with an adaptive unscented Kalman filter (AUKF) method was proposed. Experimental results indicate that it has a high level of precision and low complexity. Ref. [24] proposed a novel recursive neural network for SOC estimation. The validity and superiority were validated. In Refs. [25,26], the LSTM algorithms were improved and applied to the estimation of the SOHs of LIBs, and a high degree of estimation accuracy was obtained, which had a certain practical value. A joint LSTM and EKF method with wide temperature adaptation

was proposed in Ref. [27] which not only reduced the training time but also improved the estimation accuracy. As can be seen from the above, LSTM has become a popular method for parameter estimations of LIBs.

With the aging of a LIB, not only should the accuracy of parameter estimation be improved but the adaptability of the parameter estimation should also be enhanced. Ref. [28] proposed an adaptive estimation method which can realize the estimations of the SOC, SOH and SOE. The adaptability and precision were verified via BMS. Ref. [29] proposed a method for a hybrid model of GRU and AUKF, which had a good SOC effect and improved the efficiency and convergence rate. There are more independent adaptive estimation methods for the SOE and SOC [2,30,31], while there are fewer adaptive algorithms for combined estimations and even fewer for the SOEs and SOCs for EULIBs. Since the Ohmic internal resistance (OIR), actual energy (AE) and actual capacity (AC) parameters of a LIB are all changed to varying degrees in the step, a real-time estimation is needed in the algorithm estimation process to improve model parameters. In addition, due to the stepwise use of batteries, the initial values of the SOE or SOC have different degrees of error compared with the real values, so the model must have self-adaptation characteristics.

To ensure safety and reliability, the performance of a EULIB must be accurately reflected. This article presents a method of a combined estimation of the SOE and SOC which not only has a high level of precision but is also has adaptability.

A combined estimation method for the SOE and SOC values of echelon-use lithium-ion battery is established. The original contributions are as follows.

(1) Aimed at EULIBs, a TRCEM is established for a combined estimation of the SOE and SOC which provides reference for the promotion of the EULIB.

(2) In the process of estimating the parameters of the EULIB, LSTM is used to optimize the OIR, AE and AC and further improve the accuracy of the model.

(3) With the degradation of the EULIB, initial values of the SOE and SOC are not clear, so estimations of the EULIB parameters are discussed.

2. SOE Estimation

2.1. SOE

The EULIB's SOE is defined as the ratio of the remaining energy to the maximum available energy, as shown in the following equation:

$$S_{ek+1} = S_{ek} - \frac{U_k \Delta t}{E} i_k \quad (1)$$

where S_{ek} and S_{ek+1} are the EULIB's SOE at times k and $k + 1$; E is the EULIB's energy; i_k is the EULIB's current at time k ; U_k is the EULIB's WV at time k ; and Δt is the sampling time.

2.2. SOC

The EULIB's SOC is defined as the ratio of the remaining capacity to the maximum available capacity, as shown in equation [32]:

$$S_{ck+1} = S_{ck} - \frac{\Delta t}{C} i_k \quad (2)$$

where S_{ck} and S_{ck+1} are EULIB's SOC at times k and $k + 1$; and C is the EULIB's capacity.

2.3. SOE and SOC Estimation Model Based on TRCEM

Due to the complex, nonlinear system of a EULIB, to simulate the characteristics of a EULIB more accurately, a higher-order model must be selected. After considering accuracy, complexity and practical value, the TRCEM was adopted.

According to Figure 2, U_{oc} is the EULIB's open circuit voltage (OCV); U_L is the EULIB's WV; R_0 is the EULIB's OIR; R_1 and C_1 are the ohmic polarization resistance and capacitance; R_2 and C_2 are the electrochemical polarization internal resistance and capacitance; R_3 and C_3 are the internal resistance and capacitance of concentration difference polarization; U_1 ,

U_2 and U_3 are the voltages at both ends of capacitors C_1 , C_2 and C_3 respectively; i_L is the charge/discharge current; and $\tau_1 = R_1 C_1$, $\tau_2 = R_2 C_2$, and $\tau_3 = R_3 C_3$ are time constants.

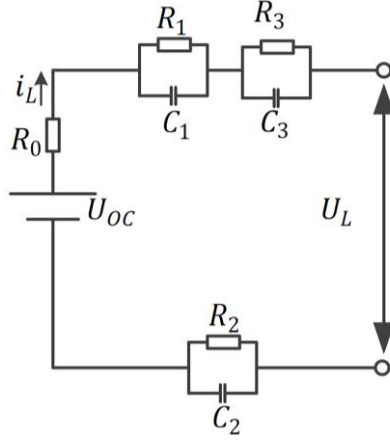


Figure 2. The TRCEM of an SOE and SOC estimation.

As shown in Figure 2, the state and observation equation of a EULIB's TRCEM are as follows:

$$\begin{bmatrix} S_{ek+1} \\ S_{ck+1} \\ U_{k+1}^{R_1 C_1} \\ U_{k+1}^{R_2 C_2} \\ U_{k+1}^{R_3 C_3} \end{bmatrix} = \begin{bmatrix} 1 & 0 & 0 & 0 \\ 1 & 0 & 0 & 0 \\ 0 \exp\left(-\frac{\Delta t}{\tau_1}\right) & 0 & 0 & 0 \\ 0 & 0 & \exp\left(-\frac{\Delta t}{\tau_2}\right) & 0 \\ 0 & 0 & 0 & \exp\left(-\frac{\Delta t}{\tau_3}\right) \end{bmatrix} \cdot \begin{bmatrix} S_{ek} \\ S_{ck} \\ U_k^{R_1 C_1} \\ U_k^{R_2 C_2} \\ U_k^{R_3 C_3} \end{bmatrix} + \begin{bmatrix} -\frac{U_k \Delta t}{E} \\ -\frac{\Delta t}{C} \\ R_1 \left(1 - \exp\left(-\frac{\Delta t}{\tau_1}\right)\right) \\ R_2 \left(1 - \exp\left(-\frac{\Delta t}{\tau_2}\right)\right) \\ R_3 \left(1 - \exp\left(-\frac{\Delta t}{\tau_3}\right)\right) \end{bmatrix} \cdot i_k + q_k \quad (3)$$

$$U_k = \left[\frac{d(U_{oc}(S_e))}{dS_e} \Big|_{S_e=S_{ek}} \quad \frac{d(U_{oc}(S_c))}{dc} \Big|_{S_c=S_{ck}} \quad -1 \quad -1 \quad -1 \right] \cdot \begin{bmatrix} S_{ek} \\ S_{ck} \\ U_k^{R_1 C_1} \\ U_k^{R_2 C_2} \\ U_k^{R_3 C_3} \end{bmatrix} - i_k R_0 + \gamma_k \quad (4)$$

$$A_k = \begin{bmatrix} 1 & 0 & 0 & 0 \\ 1 & 0 & 0 & 0 \\ 0 \exp\left(-\frac{\Delta t}{\tau_1}\right) & 0 & 0 & 0 \\ 0 & 0 & \exp\left(-\frac{\Delta t}{\tau_2}\right) & 0 \\ 0 & 0 & 0 & \exp\left(-\frac{\Delta t}{\tau_3}\right) \end{bmatrix}, B_k = \begin{bmatrix} -\frac{U_k \Delta t}{E} \\ -\frac{\Delta t}{C} \\ R_1 \left(1 - \exp\left(-\frac{\Delta t}{\tau_1}\right)\right) \\ R_2 \left(1 - \exp\left(-\frac{\Delta t}{\tau_2}\right)\right) \\ R_3 \left(1 - \exp\left(-\frac{\Delta t}{\tau_3}\right)\right) \end{bmatrix}, x_k = \begin{bmatrix} S_{ek} \\ S_{ck} \\ U_k^{R_1 C_1} \\ U_k^{R_2 C_2} \\ U_k^{R_3 C_3} \end{bmatrix}$$

$$u_k = i_k, C_k = \left[\frac{d(U_{oc}(S_e))}{dS_e} \Big|_{S_e=S_{ek}} \quad \frac{d(U_{oc}(S_c))}{dc} \Big|_{S_c=S_{ck}} \quad -1 \quad -1 \quad -1 \right]$$

So

$$f(x_k, u_k) = A_k x_k + B_k u_k \quad (5)$$

$$g(x_k, u_k) = C_k x_k - R_{0,k} u_k \quad (6)$$

where $U_k^{R_1C_1}$, $U_k^{R_2C_2}$ and $U_k^{R_3C_3}$ are the estimated voltage values of R_1 , R_2 and R_3 at time k ; q_k and γ_k are independent system noises; and $U_{oc}(S_e)$ and $U_{oc}(S_c)$ are the OCV values corresponding to the value of the EULIB's SOE and SOC.

2.4. Model Parameter Identification

A EULIB's parameters, such as U_L , i_L , U_{OC} and R_0 , are identified via the least square method, which will not be repeated in this article. For specific methods, please refer to Ref. [33].

2.5. SOE and SOC Estimation Based on AEKF

From Formulas (4) and (5), the state and observation formulas are as follows:

$$x_{k+1,E} = f(x_{k,E}, u_{k,E}, \theta_{k,E}) + q_{k,E} \quad (7)$$

$$y_{k+1,E} = g(x_{k,E}, u_{k,E}, \theta_{k,E}) + \gamma_{k,E} \quad (8)$$

where $\theta_{k,E}$ is the state variable's OIR, AE and AC, $\theta_{k,E} = [R_{0,k,E}, E_{k,E}, C_{k,E}]^T$; $u_{k,E}$ is the current of the EULIB, which is the input variable of the system; $y_{k,E}$ is the WV of the EULIB, which is the observation variable of the system. $q_{k,E}$ and $\gamma_{k,E}$ are zero-mean Gaussian white noises, and their error covariance matrices are $Q_{k,E}$ and $R_{k,E}$, respectively.

The adaptive extended Kalman filter (AEKF) algorithm flows as follows:

- Step 1: Initialize $x_{k,E}$:

$$\hat{x}_{0,E} = E(x_{0,E}) \quad (9)$$

$$\hat{P}_{0,E} = E(x_{0,E} - \hat{x}_{0,E})(x_{0,E} - \hat{x}_{0,E})^T \quad (10)$$

- Step 2: Time update $x_{k,E}$:

Estimation of the state variable:

$$x_{k,E} = f(\hat{x}_{k-1,E}, u_{k-1,E}) \quad (11)$$

- Estimation of the error covariance:

$$P_{k,E} = A_{k-1,E} \hat{P}_{k-1,E} A_{k-1,E}^T + Q_{k,E} \quad (12)$$

- Step 3: Status update $x_{k,E}$:

Kalman gain:

$$K_{k,E} = P_{k,E} C_{k,E}^T (C_{k,E} P_{k,E} C_{k,E}^T + R_{k,E})^{-1} \quad (13)$$

Optimal estimation of the state variable:

$$\hat{x}_{k,E} = x_{k,E} + K_{k,E} [y_{k,E} - g(\hat{x}_{k-1,E}, u_{k-1,E})] \quad (14)$$

Optimal estimation of the covariance:

$$\hat{P}_{k,E} = (E - K_{k,E} C_{k,E}) P_{k,E} \quad (15)$$

- Step 4: Process noise covariance:

$$Q_{k,E} = (1 - d_{k,E}) Q_{k-1,E} + d_{k,E} [K_{k,E} (\hat{y}_{k,E} - y_{k,E}) (\hat{y}_{k,E} - y_{k,E})^T K_{k,E}^T + P_{k,E} - A_{k-1,E} \hat{P}_{k-1,E} A_{k-1,E}^T] \quad (16)$$

- Step 5: Observation noise covariance:

$$R_{k,E} = (1 - d_{k,E}) R_{k-1,E} + d_{k,E} [(\hat{y}_{k,E} - y_{k,E}) (\hat{y}_{k,E} - y_{k,E})^T - C_{k,E} P_{k,E} C_{k,E}^T] \quad (17)$$

where $d_{k,E} = \frac{1-b_E}{1-b_E^k}$, $k = 1, 2, \dots, n$, b_E is forgetting factor, $0 < b_E < 1$; $y_{k,E}$ is the estimated value at k time; and $\hat{y}_{k,E}$ is the actual observation value at time k .

According to Formulas (3), (4) and (14):

$$\hat{x}_{k,E} = \begin{bmatrix} \hat{S}_{ek,E} \\ \hat{S}_{ck,E} \\ \hat{U}_{k,E}^{R_1 C_1} \\ \hat{U}_{k,E}^{R_2 C_2} \\ \hat{U}_{k,E}^{R_3 C_3} \end{bmatrix} \quad (18)$$

where $\hat{S}_{ek,E}$ and $\hat{S}_{ck,E}$ are the optimal values of the SOE and SOC, identified via the AEKF.

2.6. OIR, AE, and AC Estimation Based on AEKF

The state and observation equations of the system with the newly added state parameters are as follows:

$$\theta_{k+1,E} = \theta_{k,E} + q_{\theta,k,E} \quad (19)$$

$$D_{k+1,E} = g(x_{k,E}, u_{k,E}, \theta_{k,E}) + \gamma_{\theta,k,E} \quad (20)$$

where $q_{\theta,k,E}$ and $\gamma_{\theta,k,E}$ are zero-mean Gaussian white noises and their error covariance matrices are $Q_{\theta,k,E}$ and $R_{\theta,k,E}$, respectively. By optimizing the error between the actual and the estimated values of the WV, the estimation accuracy is further improved.

The AEKF algorithm flow:

- Step 1: Initialize $\theta_{k,E}$:

$$\hat{\theta}_{0,E} = E(\theta_{0,E}) \quad (21)$$

$$P_{\theta,0,E} = E[(x_{0,E} - \hat{x}_{0,E})(x_{0,E} - \hat{x}_{0,E})^T] \quad (22)$$

- Step 2: Time update $\theta_{k,E}$:

Estimation of the state variable:

$$\theta_{k,E} = \hat{\theta}_{k-1,E} + q_{\theta,k,E} \quad (23)$$

- Estimation of the error covariance:

$$P_{\theta,k,E} = \hat{P}_{\theta,k-1,E} + Q_{\theta,k,E} \quad (24)$$

- Step 3: Status update $\theta_{k,E}$:

Kalman gain:

$$K_{\theta,k,E} = P_{\theta,k,E} C_{\theta,k,E}^T (C_{k,E} P_{\theta,k,E} C_{k,E}^T + R_{\theta,k,E})^{-1} \quad (25)$$

Optimal estimation of the state variable:

$$\hat{\theta}_{k,E} = \theta_{k,E} + K_{\theta,k,E} [y_{k,E} - \hat{y}_{k,E}] \quad (26)$$

Optimal estimation of the covariance:

$$\hat{P}_{\theta,k,E} = P_{\theta,k,E} - K_{\theta,k,E} P_{\theta,k,E} K_{\theta,k,E}^T \quad (27)$$

- Step 4: Process noise mean and covariance:

$$q_{\theta,k,E} = (1 - d_{\theta,k,E}) q_{\theta,k-1,E} + d_{\theta,k,E} [\hat{\theta}_{k,E} - \theta_{k,E}] \quad (28)$$

$$Q_{\theta,k,E} = (1 - d_{\theta,k,E})Q_{\theta,k-1,E} + d_{\theta,k,E}[K_{\theta,k,E}(\hat{y}_{k,E} - y_{k,E})(\hat{y}_{k,E} - y_{k,E})^T K_{\theta,k,E}^T + P_{\theta,k,E} - A_{k-1,E}\hat{P}_{\theta,k-1,E}A_{k-1,E}^T] \quad (29)$$

- Step 5: Observation noise covariance:

$$R_{\theta,k,E} = (1 - d_{\theta,k,E})R_{\theta,k-1,E} + d_{\theta,k,E}[(\hat{y}_{k,E} - y_{k,E})(\hat{y}_{k,E} - y_{k,E})^T - C_{k,E}P_{\theta,k,E}C_{k,E}^T] \quad (30)$$

where $d_{\theta,k,E} = \frac{1-b_{\theta,E}}{1-b_{\theta,E}^k}$, b_θ is the forgetting factor of θ , $0 < b_{\theta,E} < 1$.

2.7. Optimize the OIR, AE, and AC Based on LSTM

To further improve the precision of the SOE and SOC estimation, this article adopts LSTM to optimize the OIR, AE, and AC in the Kalman filter process. The LSTM algorithm is a special type of recursive neural network which has been widely used. LSTM algorithm includes forget, input and output gates to ensure long-term time dependence [34], as shown in Figure 3.

$$f_k = \sigma(b_f + \omega_{f,\hat{\theta}}\hat{\theta}_{k-1,E} + \omega_{f,\theta}\theta_{k,E}) \quad (31)$$

$$i_k = \sigma(b_i + \omega_{i,\hat{\theta}}\hat{\theta}_{k-1,E} + \omega_{i,\theta}\theta_{k,E}) \quad (32)$$

$$\tilde{c}_k = \tanh(\omega_{c,\theta}\theta_{k,E} + \omega_{c,\hat{\theta}}\hat{\theta}_{k-1,E} + b_c) \quad (33)$$

$$c_k = c_{k-1} * f_k + i_k * \tilde{c}_k \quad (34)$$

$$o_k = \sigma(b_o + \omega_{o,\hat{\theta}}\hat{\theta}_{k-1,E} + \omega_{o,\theta}\theta_{k,E}) \quad (35)$$

$$\hat{\theta}_{k,E} = o_k * \tanh(c_k) \quad (36)$$

where $\theta_{k,E}$ and $\hat{\theta}_{k,E}$ are the input and output data at time k , and c_k is the status of the memory cell at time k . f_k , i_k , and o_k are the forget, input and output gates. Additionally, σ is the sigmoid function, and $*$ is the element-wise product. ω and b are the weight matrices and the bias vectors, respectively.

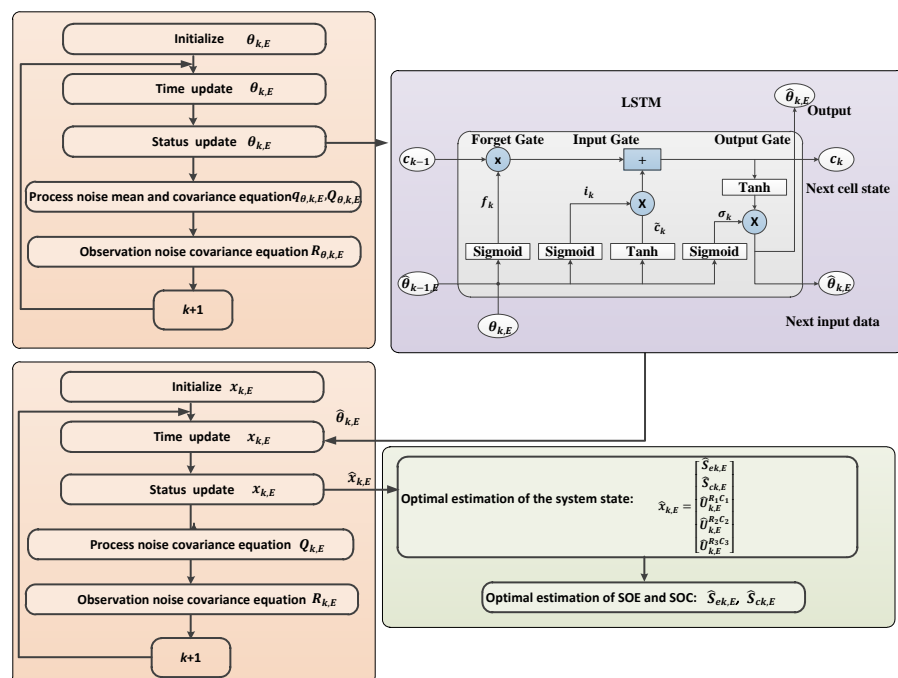


Figure 3. Flow chart.

In this article, the main parameters of the LSTM model are as follows: 3 input layer variables; 3 output layer variables; 150 hidden layer units; 1 hidden layer; 100 epochs; and an adjustable parameter, batch_size, of 128.

2.8. SOE Estimation Based on AEKF and LSTM

An SOE and SOC estimation flow chart of a EULIB via AEKF and LSTM is shown in Figure 3.

3. Simulation

3.1. Experiment

A charge and discharge experiment of an LIB was carried out at room temperature using the test equipment (BTS20), as shown in Figure 4 and Table 1 [35].

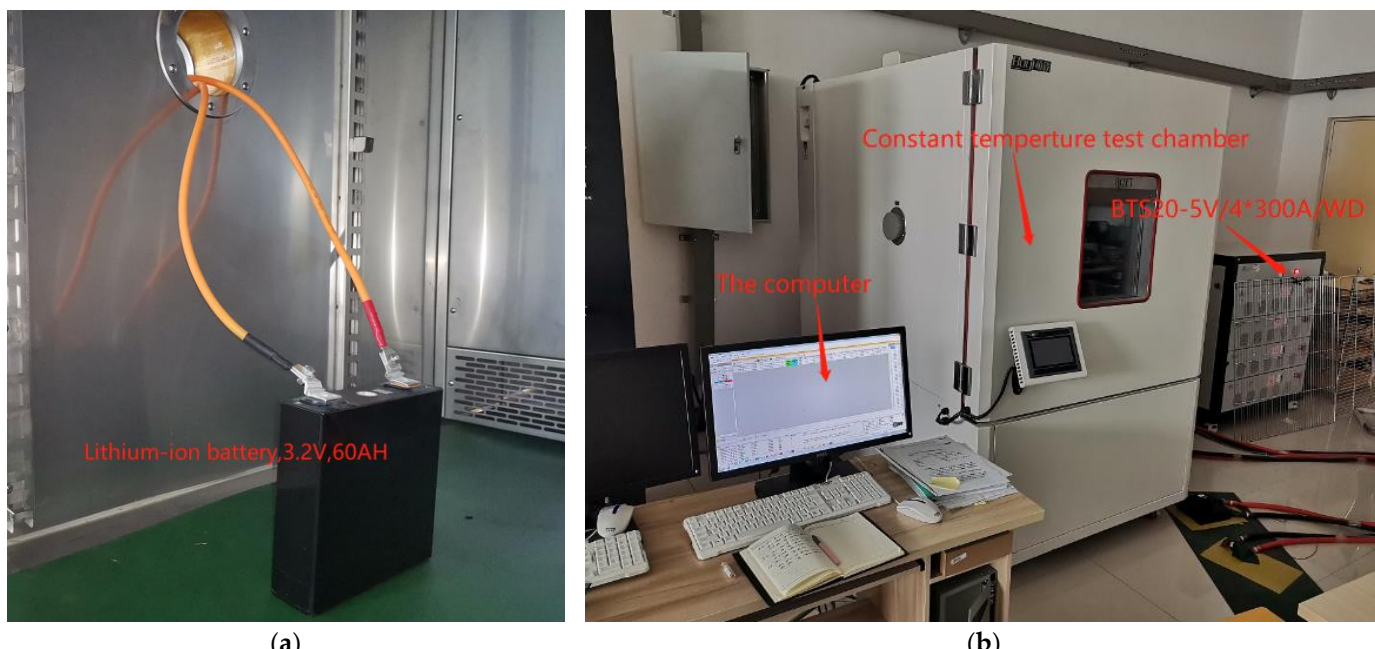


Figure 4. Testing system. (a) LIB. (b) Experimental equipment.

Table 1. LIB parameters.

Items	Parameter	Remarks
Rated capacity	60 Ah	60 A
Rated voltage	3.2 V	
Cut-off voltage	2.5 V	
Rated energy	192 Wh	Watt-Hour
Maximum charging voltage	3.65 V	
Maximum continuous charge current	20 A	0.3 C
Charging/discharging temperature	25 °C	

In this paper, a 1C current was used to charge and discharge the LIB attenuation cycle experiment. In the process of battery decay from a “new battery” to a “EULIB”, the estimation of the SOC and SOE of the LIB was studied, and the comparison was made to verify and analyze the battery parameters that reflected the state and actual performance of the battery.

To simulate the working conditions better, discharge experiments on a fully charged EULIB were carried out with different currents. MATLAB R2022a was used for simulation verification.

The data when the LIB degradation reached 90%, 60%, and 30% were selected, and the combined estimation method based on MATLAB was verified. When 90% was selected, the battery was in a normal service state for verifying the combined estimation method,

which represented the accuracy and convergence of the normal service period estimation method. When 60% was selected, the battery was in the step echelon-use state, and the combined estimation method was further verified, which represented the estimation of the step echelon-use period. When 30% was selected, the battery was at the critical value of scrap, which was representative to a certain extent.

In this article, the initial values of the SOE and SOC are changed to 100%, 60% and 20% separately, and the results are discussed. During simulation, the estimated values were calculated via the AEKF and LSTM algorithm, and the actual values were acquired based on the BTS20.

From Equation (18), the SOE error of the AEKF and LSTM formula is as follows:

$$\text{SOE error of AEKF} = \hat{S}_{ek,E} - S_{actual} \quad (37)$$

where S_{actual} is the value acquired by the BTS20, and energy is used for representation in this paper.

The SOC error of the AEKF and LSTM formula is as follows:

$$\text{SOC error of AEKF} = \hat{S}_{ck,E} - S_{actual} \quad (38)$$

3.2. Decayed to 90%

When the capacity decayed to 90%, the SOE and SOC values starting at 100%, 60% and 20% are shown in Figure 5.

As shown in Figure 5(a2–c2), the top and bottom graphs are observation noise covariance (ONC) and process noise covariance (PNC) curves, respectively. During the first 1500 s period, the curves fluctuate greatly, which is an adaptive adjustment. After the second 1500 s period, the fluctuation tends to be stable, and the error gradually approaches zero. The curves show that the method is convergent. With the increase in the error between the initial and true values of the SOE or SOC, the covariance of both the observed value and the process noise increases. Even if the initial value is different, the actual value can be tracked eventually through the adjustment of the algorithm.

As shown in Figure 5(a1–c1), the top and bottom graphs are adaptive and error curves, respectively. According to Table 2 and Figure 5, the SOE error ranges from -0.85% to 0.96% , and the SOC error ranges from -0.88% to 0.93% . There is little difference in the estimated error between the SOC and SOE no matter how much difference exists between the initial and real values, which can reflect the state performance of a lithium battery.

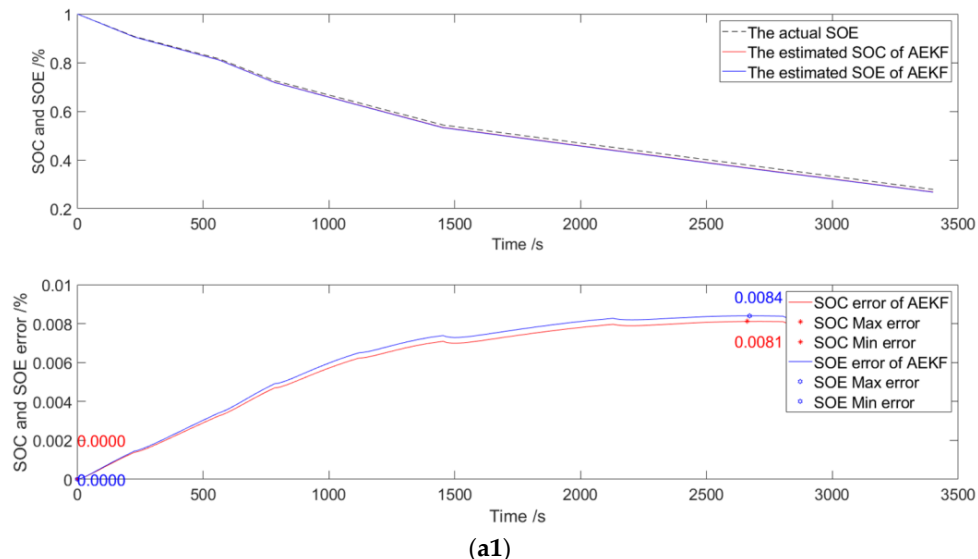
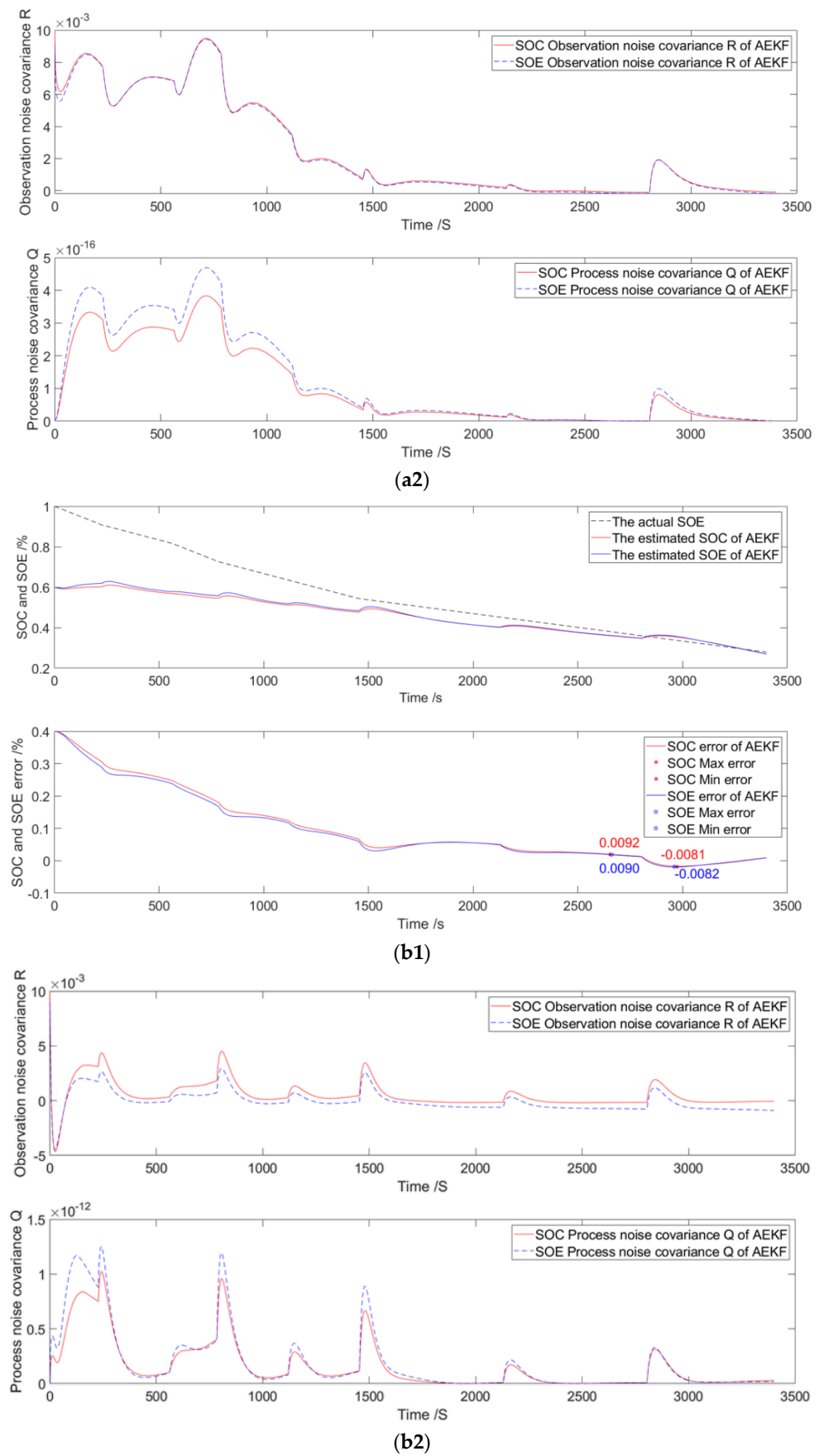


Figure 5. Cont.

**Figure 5. Cont.**

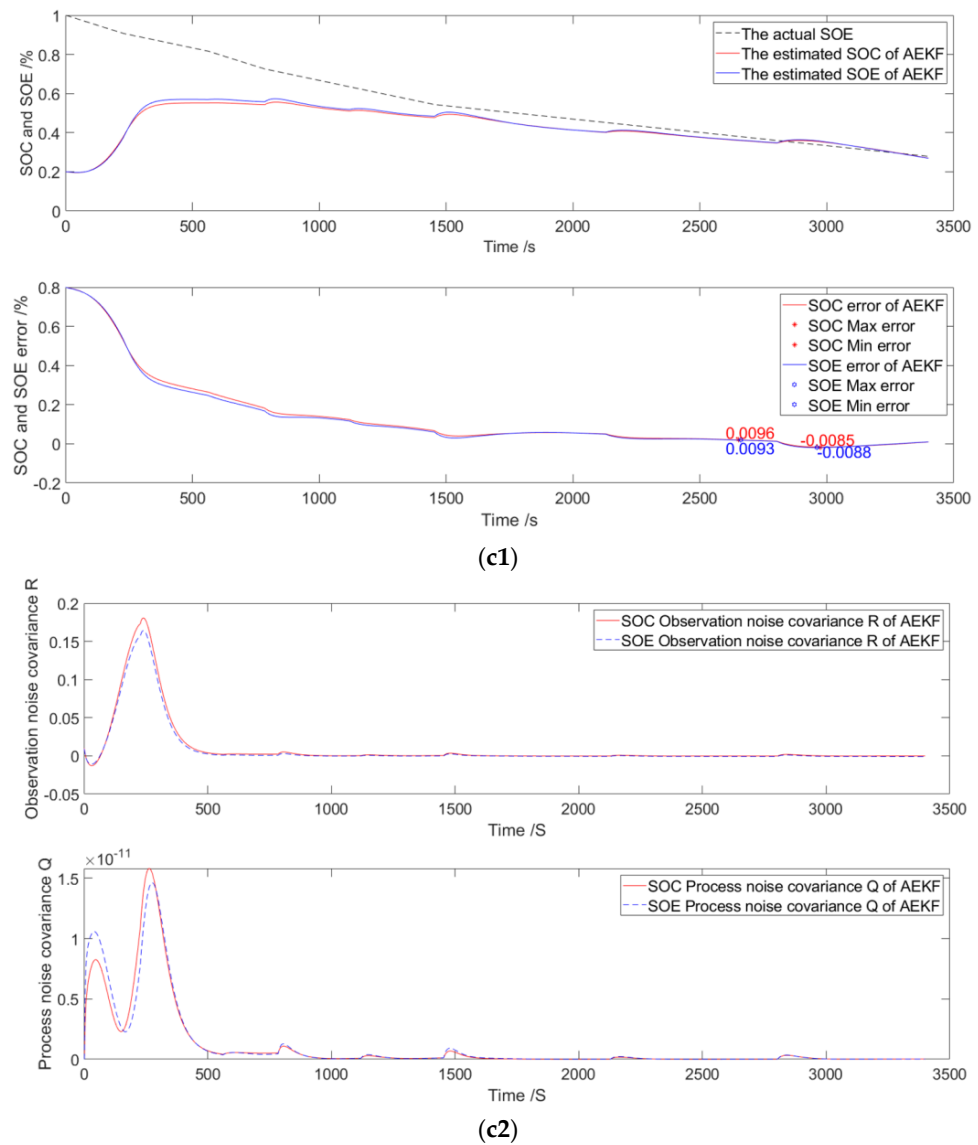


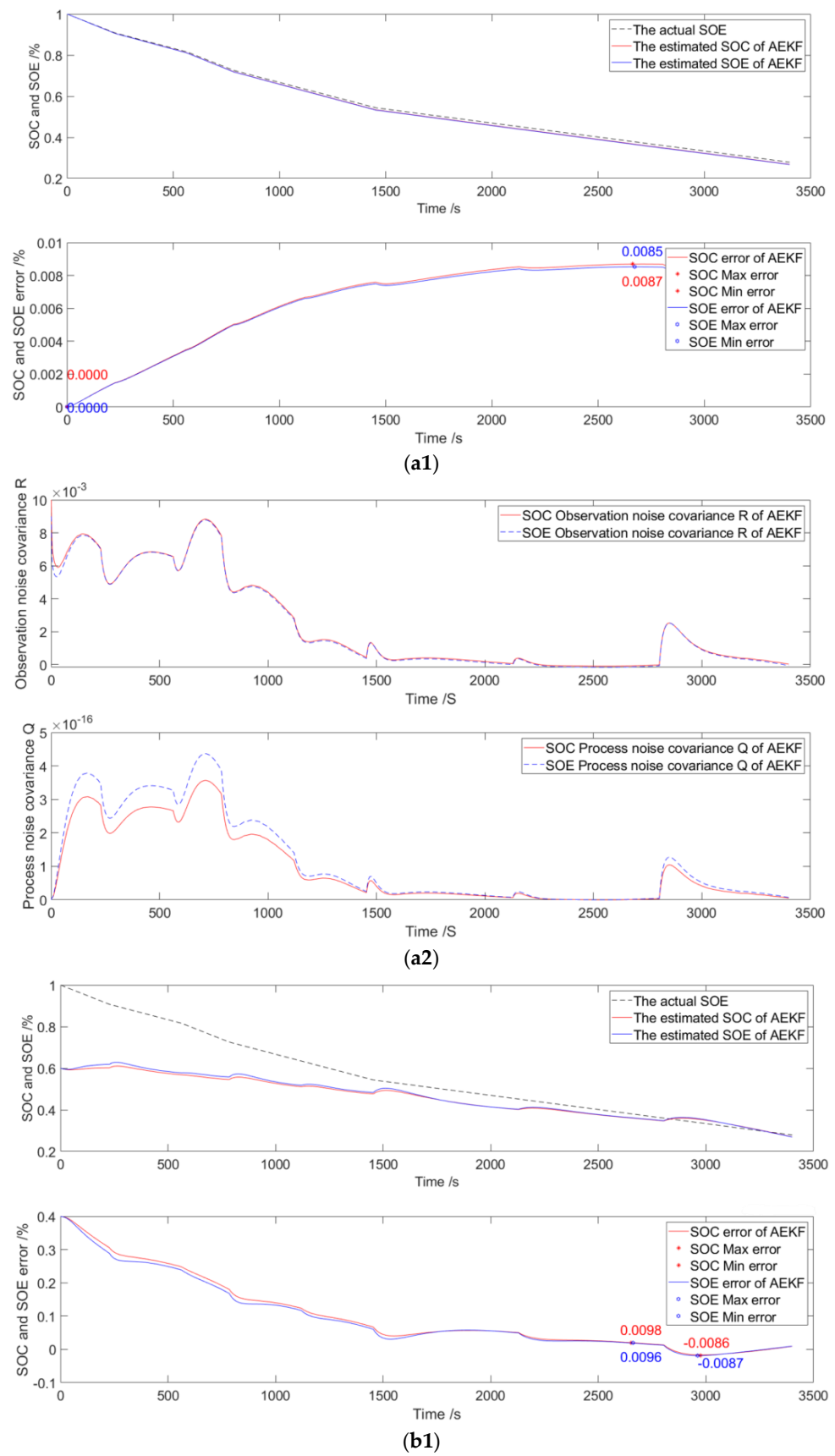
Figure 5. The validation curves when the capacity decayed to 90%, with the SOE and SOC starting at 100%, 60% and 20%. (a1–c1) Are curves of estimation and error, and (a2–c2) are curves of ONC (R) and PNC (Q).

Table 2. Estimation errors of a LIB's SOE and SOC.

	Initial Value	SOE Error	SOC Error
Decayed to 90%	100%	0% to 0.84%	0% to 0.81%
	60%	−0.82% to 0.90%	−0.81% to 0.92%
	20%	−0.88% to 0.93%	−0.85% to 0.96%
Decayed to 60%	100%	0% to 0.85%	0% to 0.87%
	60%	−0.87% to 0.96%	−0.86% to 0.98%
	20%	−0.92% to 0.97%	−0.89% to 1.00%
Decayed to 30%	100%	0% to 0.92%	0% to 0.94%
	60%	−1.01% to 1.11%	−1.00% to 1.14%
	20%	−1.09% to 1.16%	−1.06% to 1.19%

3.3. Decayed to 60%

When the capacity decayed to 60%, the SOE and SOC values starting at 100%, 60% and 20% are shown in Figure 6.

**Figure 6. Cont.**

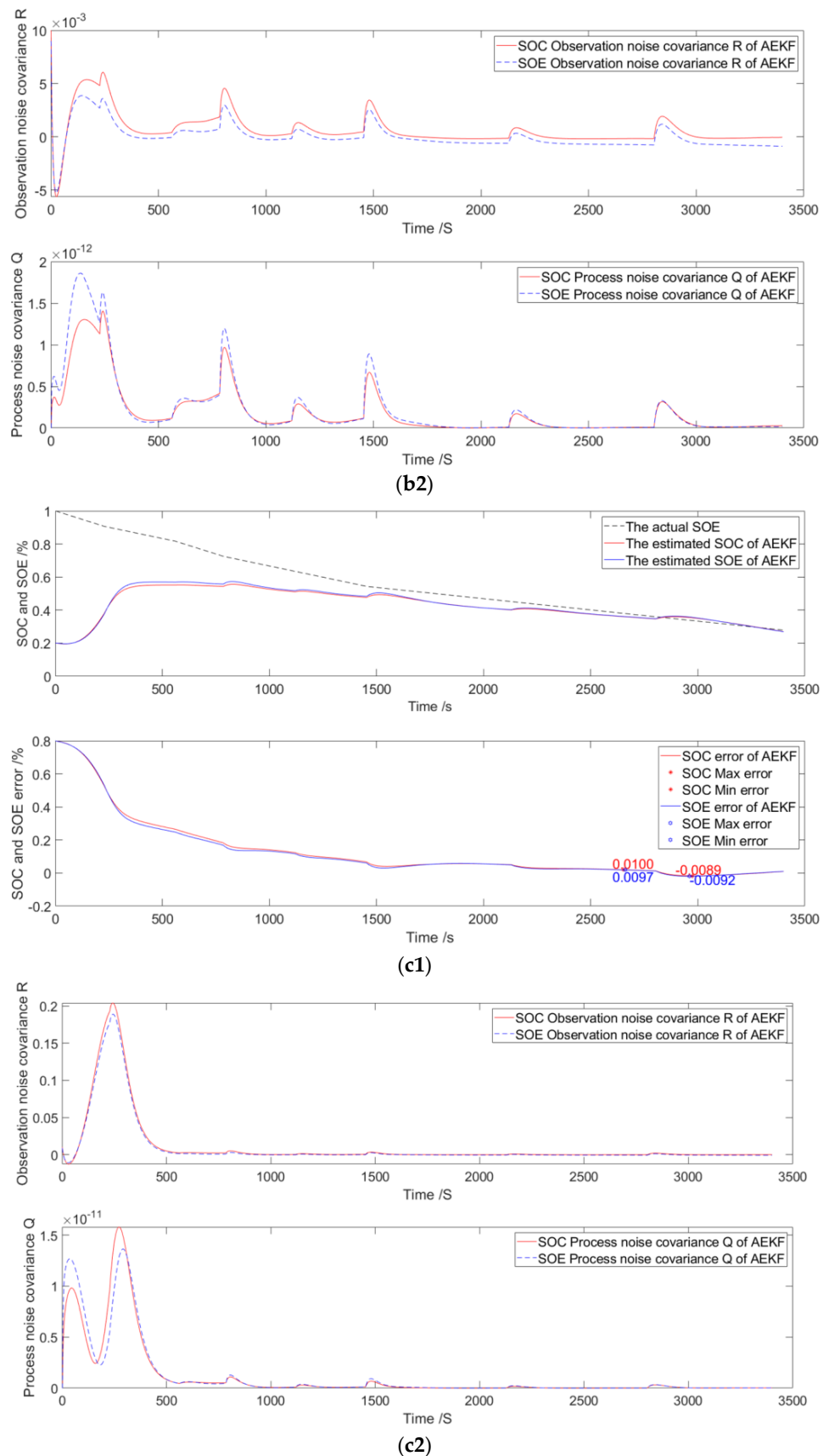


Figure 6. The validation curves when capacity decayed to 60%, with SOE and SOC values starting at 100%, 60% and 20%. **(a1–c1)** Are curves of estimation and error; **(a2–c2)** are curves of ONC (R) and PNC (Q).

As shown in Figure 6(a1–c1), the top and bottom graphs are adaptive and error curves, respectively. According to Table 2 and Figure 6, the SOE error ranges from -0.92% to 0.97% , and the SOC error ranges from -0.89% to 1.00% . As the LIB enters the stage of step echelon use, the estimation errors of the SOC and SOE begin to increase. When there is no degradation, the errors of the SOC and SOE are not much different, and the error accuracy of the SOC is higher. When the degradation began, the error accuracy of the SOE was even higher.

As shown in Figure 6(a2–c2), the top and bottom graphs are ONC and PNC curves, respectively. During the first 1500S period, the curves fluctuate greatly and are adjusted adaptively. After the second 1500S period, the fluctuation tends to be stable, and the error gradually approaches zero. The curves show that the method is convergent. In the absence of degradation, the combined estimation method is less adjusted. When degradation begins, the adjustment of the combined estimation method increases. Even if the initial value is different, the actual value can be tracked eventually through an adjustment of the algorithm.

3.4. Decayed to 30%

When the capacity decayed to 30%, the SOE and SOC values starting at 100%, 60% and 20% are shown in Figure 7. In this state, lithium batteries are at the end of the stage of echelon use, and the next step is to scrap the batteries and recycle their materials.

As shown in Figure 7(a1–c1), the top and bottom graphs are adaptive and error curves, respectively. According to Table 2 and Figure 7, the SOE error ranges from -1.09% to 1.16% , and the SOC error ranges from -1.06% to 1.19% . As the EULIB enters the end of the stage of step echelon use, the estimation errors of the SOC and SOE increase further.

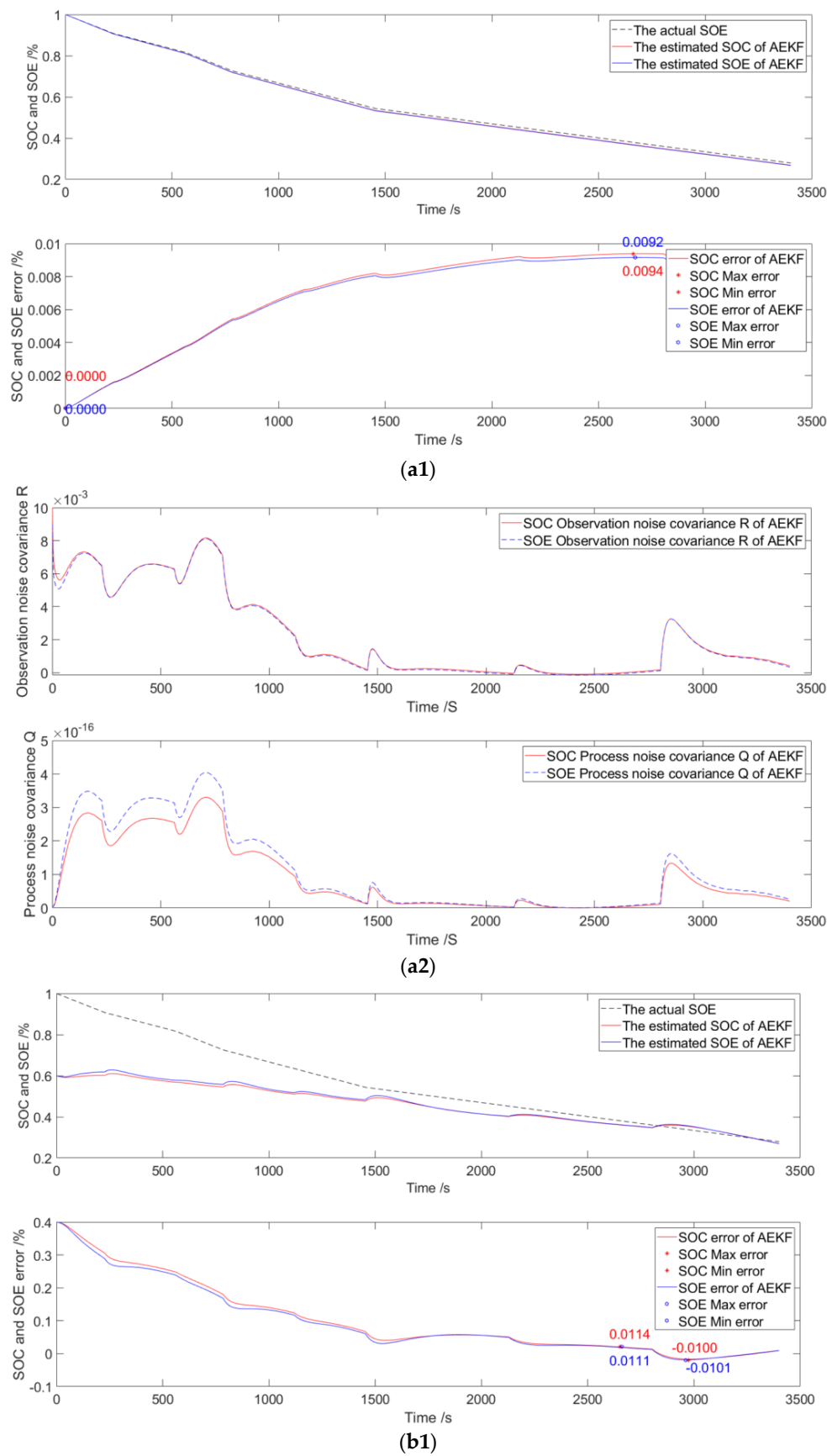
As shown in Figure 7(a1–c1), the top and bottom graphs are ONC and PNC curves, respectively. During the first 1500S period, the curves fluctuate greatly and are adjusted adaptively. After the second 1500S period, the fluctuation tends to be stable, and the error gradually approaches zero, indicating that the method is convergent. With the continuous expansion of a EULIB's degradation, the adjustment of the combined estimation method is further intensified. Even if the initial value is different, the actual value can be tracked eventually through an adjustment of the algorithm.

3.5. Discussion

According to the above, the estimation errors of an SOE and SOC are less than 1.19% when using LSTM optimization and an AEKF. According to Table 3, compared with the accuracies of 2.34% in Ref. [2], 2% in refs. [23,28], 1.93% in ref. [36] and 1.8% in Ref. [37], the method has a high level of precision. In addition, the combination method is self-adaptive.

Table 3. Comparison of optimization methods.

Reference	Accuracy of Estimation	Adaptability	Method
Method in this paper [2]	1.19% 2.34%	Yes Yes	LSTM optimization AEKF AUKF
[23]	2%	Yes	Adaptive double fractional-order extended Kalman filter
[28]	2%	No	Interacting multiple model
[36]	1.93%	Yes	Fuzzy adaptive cubature Kalman filtering
[37]	1.8%	No	Unscented particle filter

**Figure 7. Cont.**

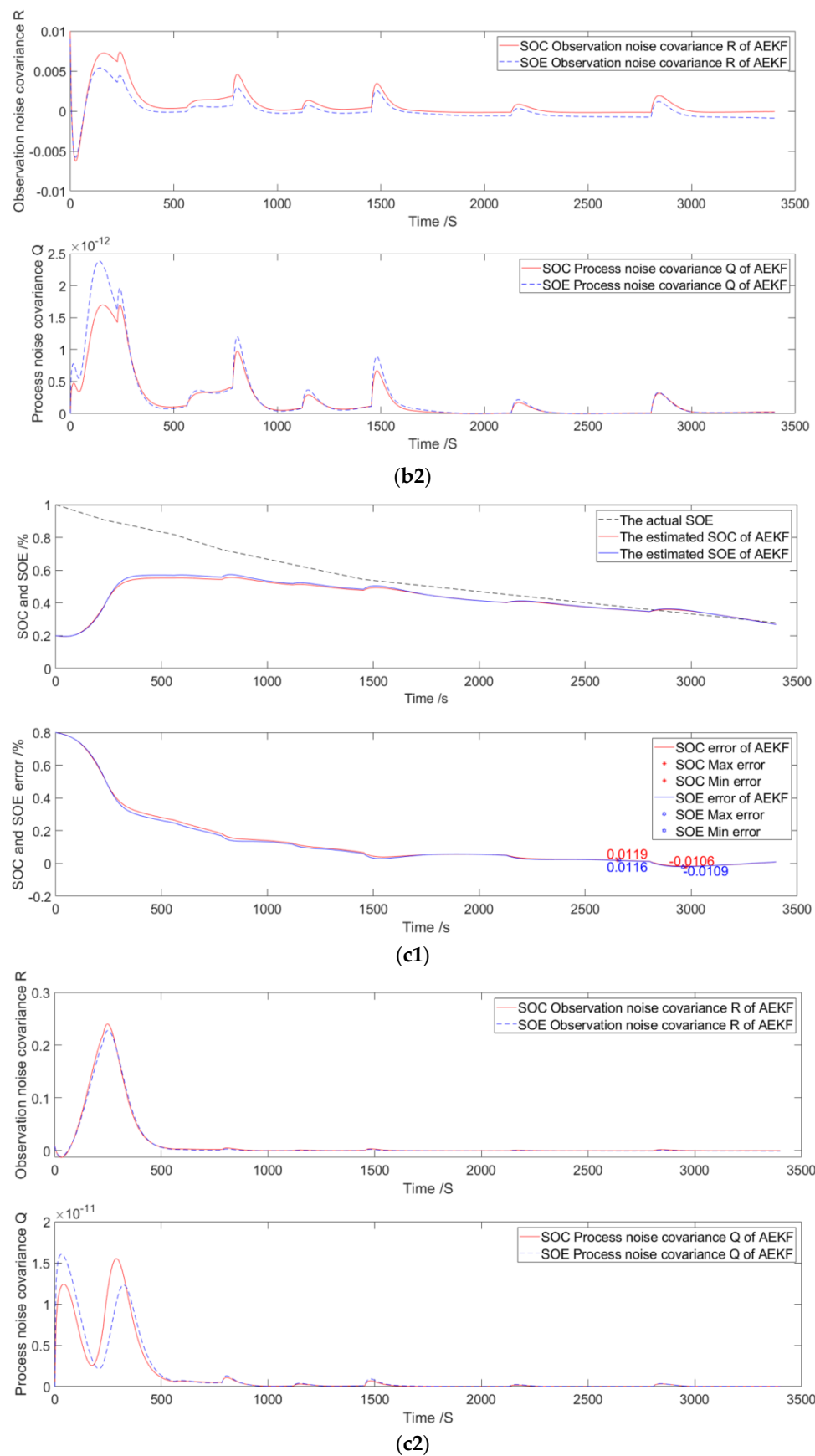


Figure 7. The validation curves when capacity decayed to 30%, with SOE and SOC starting at 100%, 60% and 20%. **(a1–c1)** Are curves of estimation and error; **(a2–c2)** are curves of ONC (R) and PNC (Q).

As lithium-ion batteries degrade, the errors in SOE and SOC estimates increase, according to Table 4. Taking the initial value of 60% as an example, when the lithium-ion battery degenerates to 90%, 60% and 30%, the maximum errors of the SOE estimation were 0.90%, 0.96% and 1.11% respectively. The maximum estimated errors of the SOC were 0.92%, 0.98% and 1.14%, respectively.

Table 4. Estimation error when starting at 60%.

Initial Value		SOE Error	SOC Error
Decayed to 90%	60%	−0.82% to 0.90%	−0.81% to 0.92%
Decayed to 60%	60%	−0.87% to 0.96%	−0.86% to 0.98%
Decayed to 30%	60%	−1.01% to 1.11%	−1.00% to 1.14%

4. Conclusions

In this article, a combined SOE and SOC estimation method based on LSTM optimization and an AEKF is established. LSTM is introduced to optimize the OIR, AE and AC parameters to improve the accuracy of the SOE and SOC estimation, and a TRCEM of a EULIB is established. Then, during the estimation of the SOE and SOC, the observation noise and process noise equations are updated iteratively to make adaptive corrections and enhance the adaptive ability. Through simulation, the EULIB capacity was decayed to 90%, 60% and 30% of its rated capacity, and even with a large initial error, the method can track the actual value. The estimation error is less than 1.19% when using LSTM optimization with an AEKF, and the method has a high level of precision.

Author Contributions: Y.Z. and E.H.; methodology, Z.W. (Zhen Wang); software, E.H.; validation, E.H., Z.W. (Zhixue Wang), and X.Z.; formal analysis, Z.W. (Zhen Wang); investigation, Z.W. (Zhen Wang); resources, Y.Z.; data curation, E.H.; writing—original draft preparation, E.H.; writing—review and editing, X.Z.; visualization, X.Q.; supervision, Z.W. (Zhixue Wang); project administration, Z.W. (Zhixue Wang); funding acquisition, Y.Z. All authors have read and agreed to the published version of the manuscript.

Funding: This work was supported by the Science and Technology Major Project of Inner Mongolia Au-tonomous Region (2020ZD0014).

Institutional Review Board Statement: Not applicable.

Informed Consent Statement: Not applicable.

Data Availability Statement: This research was conducted within the University of Shandong Jiao Tong, supported by the charging-discharging equipment (BTS20, 5V/4*300A/WD). We are thankful to the testing and simulation team members for their support with the experiment.

Conflicts of Interest: The authors declare no conflict of interest.

References

- Qiao, X.; Wang, Z.; Hou, E.; Liu, G.; Cai, Y. Online Estimation of Open Circuit Voltage Based on Extended Kalman Filter with Self-Evaluation Criterion. *Energies* **2022**, *15*, 4373. [[CrossRef](#)]
- Hou, E.; Xu, Y.; Qiao, X.; Liu, G.; Wang, Z. Research on State of Power Estimation of Echelon-Use Battery Based on Adaptive Unscented Kalman Filter. *Symmetry* **2022**, *14*, 919. [[CrossRef](#)]
- Xu, W.; Xu, J.; Lang, J.; Yan, X. A Multi-Timescale Estimator for Lithium-Ion Battery state of Charge and State of Energy Estimation Using Dual H infinity Filter. *IEEE Access* **2019**, *7*, 181229–181241. [[CrossRef](#)]
- Zhang, Y.; Li, Y.; Tao, Y.; Ye, J.; Pan, A.; Li, X.; Liao, Q.; Wang, Z. Performance assessment of retired EV battery modules for echelon use. *Energy* **2020**, *993*, 116555. [[CrossRef](#)]
- Yong, F.; Fan, B.; Chen, X.; Fengling, H. State-of-Charge and State-of-Energy Estimation for Lithium-ion Batteries Using Sliding-Mode Observers. In Proceedings of the 2021 40th Chinese Control Conference (CCC), Shanghai, China, 26–28 July 2021. [[CrossRef](#)]
- Mamadou, K.; Lemaire, E.; Delaille, A.; Riu, D.; Hing, S.E.; Bultel, Y. Definition of a State-of-Energy Indicator (SOE) for Electrochemical Storage Devices: Application for Energetic Availability Forecasting. *J. Electrochem. Soc.* **2012**, *159*, A1298–A1307. [[CrossRef](#)]

7. Barai, A.; Uddin, K.; Widanalage, W.D.; McGordon, A.; Jennings, P. The effect of average cycling current on total energy of lithium-ion batteries for electric vehicles. *J. Power Sources* **2016**, *303*, 81–85. [[CrossRef](#)]
8. Li, X.; Pan, K.; Fan, G.; Lu, R.; Zhu, C.; Rizzoni, G.; Canova, M. A physics-based fractional order model and state of energy estimation for lithium-ion batteries. Part II: Parameter identification and state of energy estimation for LiFePO₄ battery. *J. Power Sources* **2017**, *367*, 202–213. [[CrossRef](#)]
9. Wu, L.; Pang, H.; Geng, Y.; Liu, X.; Liu, J.; Liu, K. Low-complexity state of charge and anode potential prediction for lithium-ion batteries using a simplified electrochemical model-based observer under variable load condition. *Int. J. Energy Res.* **2022**, *46*, 11834–11848. [[CrossRef](#)]
10. Fan, T.E.; Liu, S.M.; Tang, X.; Qu, B. Simultaneously estimating two battery states by combining a long short-term memory network with an adaptive unscented Kalman filter. *J. Energy Storage* **2022**, *50*, 104553. [[CrossRef](#)]
11. Zhang, S.; Peng, N.; Zhang, X. An application-oriented multistate estimation framework of lithium-ion battery used in electric vehicles. *Int. J. Energy Res.* **2021**, *45*, 18554–18576. [[CrossRef](#)]
12. Shrivastava, P.; Soon, T.K.; Idris, M.Y.I.B.; Mekhilef, S.; Adnan, S.B.R.S. Combined State of Charge and State of Energy Estimation of Lithium-Ion Battery Using Dual Forgetting Factor-Based Adaptive Extended Kalman Filter for Electric Vehicle Applications. *IEEE Trans. Veh. Technol.* **2021**, *70*, 1200–1215. [[CrossRef](#)]
13. Gao, T.; Lu, W. Machine learning toward advanced energy storage devices and systems. *iScience* **2021**, *24*, 101936. [[CrossRef](#)] [[PubMed](#)]
14. Hu, X.; Li, S.E.; Yang, Y. Advanced Machine Learning Approach for Lithium-Ion Battery State Estimation in Electric Vehicles. *IEEE Trans. Transp. Electrif.* **2016**, *2*, 140–149. [[CrossRef](#)]
15. Hossain, L.M.S.; Hannan, M.A.; Hussain, A.; Ayob, A.; Saad, M.H.M.; Karim, T.F.; How, D.N.T. Data-driven state of charge estimation of lithium-ion batteries: Algorithms, implementation factors, limitations and future trends. *J. Clean. Prod.* **2020**, *277*, 124110. [[CrossRef](#)]
16. Hu, J.N.; Hu, J.J.; Lin, H.B.; Li, X.P.; Jiang, C.L.; Qiu, X.H.; Li, W.S. State-of-charge estimation for battery management system using optimized support vector machine for regression. *J. Power Sources* **2014**, *269*, 682–693. [[CrossRef](#)]
17. Hossain Lipu, M.; Karim, T.; Ansari, S.; Miah, M.; Rahman, M.; Meraj, S.; Elavarasan, R.; Vijayaraghavan, R. Intelligent SOX Estimation for Automotive Battery Management Systems: State-of-the-Art Deep Learning Approaches, Open Issues, and Future Research Opportunities. *Energies* **2022**, *16*, 23. [[CrossRef](#)]
18. Purohit, K.; Srivastava, S.; Nookala, V.; Joshi, V.; Shah, P.; Sekhar, R.; Panchal, S.; Fowler, R.; Tran, M.K.; et al. Soft Sensors for State of Charge, State of Energy, and Power Loss in Formula Student Electric Vehicle. *Appl. Syst. Innov.* **2021**, *4*, 78. [[CrossRef](#)]
19. Wang, Y.X.; Chen, Z.; Zhang, W. Lithium-ion battery state-of-charge estimation for small target sample sets using the improved GRU-based transfer learning. *Energy* **2022**, *244*, 123178. [[CrossRef](#)]
20. Cui, Z.; Kang, L.; Li, L.; Wang, L.; Wang, K. A combined state-of-charge estimation method for lithium-ion battery using an improved BGRU network and UKF. *Energy* **2022**, *259*, 124933. [[CrossRef](#)]
21. Ma, L.; Hu, C.; Cheng, F. State of Charge and State of Energy Estimation for Lithium-Ion Batteries Based on a Long Short-Term Memory Neural Network. *J. Energy Storage* **2021**, *37*, 102440. [[CrossRef](#)]
22. Shrivastava, P.; Soon, T.K.; Idris, M.Y.I.B.; Mekhilef, S.; Adnan, S.B.R.S. Model-based state of X estimation of lithium-ion battery for electric vehicle applications. *Int. J. Energy Res.* **2022**, *46*, 10704–10723. [[CrossRef](#)]
23. Chen, L.; Wang, S.; Jiang, H.; Fernandez, C. A novel combined estimation method for state of energy and predicted maximum available energy based on fractional-order modeling. *J. Energy Storage* **2023**, *62*, 106930. [[CrossRef](#)]
24. Chen, J.; Zhang, Y.; Wu, J.; Cheng, W.; Zhu, Q. SOC estimation for lithium-ion battery using the LSTM-RNN with extended input and constrained output. *Energy* **2023**, *262*, 125375. [[CrossRef](#)]
25. Ma, Y.; Shan, C.; Gao, J.; Chen, H. A novel method for state of health estimation of lithium-ion batteries based on improved LSTM and health indicators extraction. *Energy* **2022**, *251*, 123973. [[CrossRef](#)]
26. Gong, Y.; Zhang, X.; Gao, D.; Li, H.; Yan, L.; Peng, J.; Huang, Z. State-of-health estimation of lithium-ion batteries based on improved long short-term memory algorithm. *J. Energy Storage* **2022**, *53*, 105046. [[CrossRef](#)]
27. Takyi-Aninakwa, P.; Wang, S.; Zhang, H.; Li, H.; Xu, W.; Fernandez, C. An optimized relevant long short-term memory-squared gain extended Kalman filter for the state of charge estimation of lithium-ion batteries. *Energy* **2022**, *260*, 120043. [[CrossRef](#)]
28. Rahimifard, S.; Ahmed, R.; Habibi, S. Interacting Multiple Model Strategy for Electric Vehicle Batteries State of Charge/Health/Power Estimation. *IEEE Access* **2021**, *9*, 109875–109888. [[CrossRef](#)]
29. Chen, J.; Zhang, Y.; Li, W.; Cheng, W.; Zhu, Q. State of charge estimation for lithium-ion batteries using gated recurrent unit recurrent neural network and adaptive Kalman filter. *J. Energy Storage* **2022**, *55*, 105396. [[CrossRef](#)]
30. Li, X.; Xu, J.; Hong, J.; Tian, J.; Tian, Y. State of energy estimation for a series-connected lithium-ion battery pack based on an adaptive weighted strategy. *Energy* **2021**, *214*, 118858. [[CrossRef](#)]
31. Chen, Y.; Yang, X.; Luo, D.; Wen, R. Remaining available energy prediction for lithium-ion batteries considering electrothermal effect and energy conversion efficiency. *J. Energy Storage* **2021**, *40*, 102728. [[CrossRef](#)]
32. Xia, B.; Chen, C.; Tian, Y.; Sun, W.; Xu, Z.; Zheng, W. A novel method for state of charge estimation of lithium-ion batteries using a nonlinear observer. *J. Power Sources* **2014**, *270*, 359–366. [[CrossRef](#)]

33. Hou, E.; Xu, Y.; Qiao, X.; Liu, G.; Wang, Z. State of Power Estimation of Echelon-Use Battery Based on Adaptive Dual Extended Kalman Filter. *Energies* **2021**, *14*, 5579. [[CrossRef](#)]
34. Lu, J.X.; Zhang, Q.P.; Yang, Z.H.; Tu, M.F.; Lu, J.J.; Peng, H. Short-term load forecasting method based on CNN-LSTM hybrid neural network model. *Autom. Electr. Power Syst.* **2019**, *43*, 131–137. [[CrossRef](#)]
35. Meng, J.; Yue, M.; Diallo, D. Nonlinear extension of battery constrained predictive charging control with transmission of Jacobian matrix. *Int. J. Electr. Power Energy Syst.* **2023**, *146*, 108762. [[CrossRef](#)]
36. Yang, X.; Wang, S.; Xu, W.; Qiao, J.; Yu, C.; Takyi-Aninakwa, P.; Jin, S. A novel fuzzy adaptive cubature Kalman filtering method for the state of charge and state of energy co-estimation of lithium-ion batteries. *Electrochim. Acta* **2022**, *415*, 140241. [[CrossRef](#)]
37. Wei, X.; Jun, C.; Yu, G.; Jiachen, M.; Jiaqing, C. Unscented Particle Filter Based State of Energy Estimation for LiFePO₄ Batteries Using an Online Updated Model. *Int. J. Automot. Technol.* **2022**, *23*, 503–510. [[CrossRef](#)]

Disclaimer/Publisher’s Note: The statements, opinions and data contained in all publications are solely those of the individual author(s) and contributor(s) and not of MDPI and/or the editor(s). MDPI and/or the editor(s) disclaim responsibility for any injury to people or property resulting from any ideas, methods, instructions or products referred to in the content.